ELSEVIER

Physics of the Earth and Planetary Interiors 121 (2000) 249–271

PHYSICS OF THE EARTH AND PLANETARY INTERIORS

www.elsevier.com/locate/pepi

Preliminary determination of focal mechanisms from the inversion of spectral amplitudes of mantle waves

Dominique Reymond [a], Emile A. Okal [b,*]

[a] *Laboratoire de Géophysique, Commissariat à l'Energie Atomique, Boîte Postale 640, F-98713 Papeete, Tahiti, French Polynesia*
[b] *Department of Geological Sciences, Northwestern University, Evanston, IL 60201, USA*

Received 22 January 2000; accepted 27 May 2000

Abstract

We present a method for the preliminary determination of focal mechanisms (PDFM), based on the inversion of deviatoric moment tensor components from depleted datasets of mantle wave spectral amplitudes. The latter are found to be largely insensitive to errors in epicentral estimates, which can hamper the inversion of the full complex spectrum under real-time operational conditions. Robust solutions can be obtained from Rayleigh wave spectra at as few as three stations, and from a combination of Rayleigh and Love waves at only two stations, provided they sample 60° in azimuth. The systematic application of this method to a dataset of 43 large earthquakes during 1996–1999 yielded mechanisms rotated an average of only 17° from the published Harvard CMT, a figure comparing favorably with the case of other catalogues, such as the USGS moment tensor solutions.

Keywords: Preliminary determination of focal mechanisms; Rayleigh wave; Love wave

1. Introduction and motivation

We present in this paper a method of preliminary determination of focal mechanisms (or PDFM) based on the inversion of deviatoric moment tensor components from strongly depleted datasets of surface wave spectral amplitudes at mantle periods ($T \geq 90$ s). It can be used routinely with as few as three stations, occasionally with only two. Our method is based on the early work of Romanowicz and Suárez' (1983), who demonstrated the feasibility of inverting only the spectral amplitudes of Rayleigh waves from a large dataset of stations. We generalize their results through the introduction of the Love spectra, and explore systematically the performance of the method when the dataset is depleted by a reduction in the number of stations. In the general context of tsunami warning, we are motivated in this study by the quest for a reasonably accurate description of focal mechanisms of large distant earthquakes, in real-time and with a minimal amount of data.

More complete and classical methods of moment tensor inversion (e.g. Dziewonski et al., 1981) routinely use the full complex spectrum and interpret the phase information following an adequate path correction. However, the latter requires in principle an accurate knowledge of the origin time and location of the event, and of the phase velocity along the path, to a typical accuracy of 0.5% (Patton and Aki, 1979). While the centroid of the source is routinely solved in space and time by algorithms such as Harvard's, this needs a large data space, which in turn requires some

* Corresponding author. Tel.: +1-847-491-3194; fax: +1-847-491-8060.
E-mail address: emile@earth.nwu.edu (E.A. Okal).

0031-9201/00/$ – see front matter
PII: S0031-9201(00)00171-0

combination of a large number of stations, a very broad frequency band, and a long record window ensuring the contribution of overtones and/or body phases.

A number of authors have addressed the question of the feasibility of obtaining CMT solutions from minimal datasets, using the full complex spectrum of body and mantle waves (Buland and Gilbert, 1976; Ekström et al., 1986; Dufumier and Cara, 1995; Dufumier, 1996; Huang, 1996). In the case of strongly depleted datasets, there are, however, significant advantages to using only spectral amplitudes: for example, under real-time operational conditions, the epicenter may only be estimated with a precision of a few hundred km; an error of only 150 km in epicentral distance would lead to errors of 45° in the phase correction for propagation at 240 s, and of more than 100° at 120 s. On the contrary, we will show in Section 3 that the inversion of spectral amplitudes is remarkably robust with respect to a change of epicentral location.

2. Techniques

2.1. Inversion

Our inversion method is inspired by Romanowicz and Suárez' (1983) non-linear inversion of Rayleigh wave spectral amplitudes, which builds on the work of Romanowicz (1982). We recall here briefly the principle of the method, which is based on a two-step algorithm.

In the notation of Kanamori and Stewart (1976) and Kanamori and Given (1981), the modulus $R(\omega, h; \theta)$ of the fundamental Rayleigh wave spectrum at angular frequency ω for a station located at azimuth θ from a source at depth h depends on the moment tensor components of the source, M_{kl}, through:

$$R(\omega, h; \theta) = \sqrt{R_r^2(\omega, h; \theta) + R_i^2(\omega, h; \theta)} \quad (1)$$

with the real and imaginary parts of R given by:

$$R_r(\omega, h; \theta) = \tfrac{1}{2} M_{zz} S_R(\omega, h) + \tfrac{1}{2}(M_{yy} - M_{xx}) \times P_R \cos 2\theta - M_{xy} P_R(\omega, h) \sin 2\theta \quad (2a)$$

$$R_i(\omega, h; \theta) = M_{xz} Q_R(\omega, h) \cos\theta + M_{yz} \times Q_R(\omega, h) \sin\theta \quad (2b)$$

where the excitation coefficients P_R, Q_R, S_R depend only on frequency and depth. In the present study, we use their values as computed for the Earth model PREM (Dziewonski and Anderson, 1981). We assume here a purely deviatoric source with no change of volume. Also, as a preliminary step in the data processing, the spectral amplitudes have been equalized to a common epicentral distance of 90°, in order to compensate for the effects of geometrical spreading and anelastic attenuation, the latter using the regionalized models developed by Okal and Talandier (1989, 1990).

When considering a set of observations at several stations indexed j over a range of frequencies indexed i, (1) can be rewritten

$$R_{ij}^2 = R^2(\omega_i, h; \theta_j) = [A_i \sin 2\theta_j + B_i \cos 2\theta_j]^2 + [D_i \sin\theta_j + E_i \cos\theta_j]^2 + C_i^2 \quad (3)$$

with

$$A_i = -P_R(\omega_i, h) M_{xy} \quad (4a)$$

$$B_i = \tfrac{1}{2} P_R(\omega_i, h)(M_{yy} - M_{xx}) \quad (4b)$$

$$C_i = \tfrac{1}{2} S_R(\omega_i, h) M_{zz} \quad (4c)$$

$$D_i = Q_R(\omega_i, h) M_{xz} \quad (4d)$$

$$E_i = Q_R(\omega_i, h) M_{yz} \quad (4e)$$

Romanowicz and Suárez' (1983) inversion strategy consists of solving, in a first step, for the coefficients $A_i, \ldots E_i$ at each frequency ω_i, this procedure being non-linear, and in a second step of obtaining the five independent moment tensor components through a linear least-squares inversion of the system (4). Focal depth is estimated by carrying out several inversions at distinct constrained focal depths, and retaining the depth optimizing the variance reduction. A discussion of the relative sensitivity of the various moment tensor components to depth is given in Romanowicz and Guillemant (1984).

We modify this algorithm in several respects to apply it to strongly depleted datasets. We note that Romanowicz and Suárez' non-linear first step requires at least five stations to invert for the five coefficients (4). Also, in the second step, it is well known that the dip-slip components M_{xz} and M_{yz} have excitation coefficients Q_R vanishing for asymptotically shallow source depths, leading to singularities in unconstrained

moment tensor inversions. For these reasons, we start our inversion by imposing $M_{xz}=M_{yz}=0$. This procedure not only stabilizes the inversion, but also allows in principle the use of as few as three stations. Following Frohlich and Davis (1999), we note that this gross simplification of the problem is routinely used, notably in the Harvard algorithm for small, poorly sampled events for which the full inversion of the five moment tensor components would otherwise be unstable (these solutions are recognized in the Harvard catalog from the combination of both a zero value and a zero standard deviation for the relevant components). We follow this general practice, which a number of previous workers (e.g. Kanamori and Given, 1981) have shown can lead to robust estimates of the source depth and of the strike azimuth ϕ of one fault plane. The resulting focal mechanisms are of course constrained to being pure strike-slip ($\delta=90°$; $\lambda=0$ and 180°) or pure thrust or normal faulting ($\delta=45°$; $\lambda=90$ and 270°).

Once this preliminary inversion for a degraded mechanism is performed, we proceed to release the dip-slip components M_{xz} and M_{yz}, and directly invert the entire dataset of spectral amplitudes at all individual stations and frequencies. This procedure restores a larger dimension to the data space, allowing the inversion of all five independent moment tensor components, even when using fewer than five stations. In addition, we can include Love wave spectral amplitudes, for which the counterpart to (2) is

$$L^2(\omega, h; \theta) = P_L^2(w, h)[\tfrac{1}{2}(M_{yy} - M_{xx}) \sin 2\theta + M_{xy} \cos 2\theta]^2 + Q_L^2(\omega, h) \times [M_{xz} \sin\theta - M_{yz} \cos\theta]^2 \quad (5)$$

the notation being, once again, that of Kanamori and Given (1981). The use of Love waves further increases the dimension of the data space, but remains optional.

Eqs. (2) and (5) are then combined into a general non-linear system for the five independent unknowns M_{kl}, which is solved iteratively, after injecting a trial solution, in practice the degraded mechanism obtained in the first step. The inversion can be stabilized by introducing a damping factor ε^2, leading to the use of

$$[\boldsymbol{A}^T\boldsymbol{A} + \varepsilon^2\boldsymbol{I}]^{-1} \times \boldsymbol{A}^T \quad (6)$$

rather than $[\boldsymbol{A}^T\boldsymbol{A}]^{-1} \times \boldsymbol{A}^T$, as the least-squares generalized inverse operator (e.g. Aki and Richards, 1980). The damping parameter, ε^2, is adjusted by monitoring the condition number C, defined as the square root of the ratio of extremal eigenvalues of $[\boldsymbol{A}^T\boldsymbol{A}]^{-1}$: $C^2=\lambda_{max}/\lambda_{min}$ (Tarantola, 1987). In most cases, the inversions have condition numbers of a few units, and damping is unwarranted. However, as discussed in Section 4, certain geometries have condition numbers approaching 100 or more, and warrant the introduction of a damping factor on the order of 1% of the largest eigenvalue. This procedure (Aki and Richards, 1980; p. 697) reduces the number of parameters of the model space which are effectively resolved by the inversion, usually to a value close to 3, from the initial 5. Thus, in such unfavorable cases, our approach is comparable in scope to constraining M_{xz} and M_{yz} to zero, but more general and flexible. Finally, and precisely because it amounts to keeping those two components out of the model space, damping will not improve the inversion in the case of a low angle-angle thrust fault, common among subduction events, for which these components are primordial.

In general, when the system is well-behaved and the inversion stable, the geometry of the trial solution has little if any influence on the final result. However, the first step of the inversion remains important for the determination of source depth.

It is clear from Eqs. (2) and (5) that inverting only the spectral amplitudes of Rayleigh and Love waves (as opposed to their phase) leads to a two-fold indeterminacy, noted by Romanowicz and Suárez' (1983), and inherent in the method. First, the sense of slip on the fault can be reversed, which would amount to keeping the strike and dip angles ϕ and δ, but adding 180° to the slip angle λ; or in the tensor formalism, to changing the signs of all tensor components, thus, adding π to all spectral phases. This indeterminacy can be fully lifted by the interpretation of the polarity of one or more P-wave arrivals. Second, the entire solution can also be rotated 180° in the horizontal plane, which would keep the dip and slip angles δ and λ, but add 180° to the strike; in the tensor formalism, the signs of the components M_{xz} and M_{yz} are flipped; all spectral phases would be changed to their complex conjugates. This indeterminacy cannot be formally lifted; one solution can often be considered more probable than the other by interpreting the geological context of the event, but the less probable solution cannot be excluded.

2.2. Source finiteness

As the size of the earthquake grows, the influence of source finiteness and directivity on spectral amplitudes is well-known (e.g. Ben-Menahem, 1961) and must be discussed. According to general scaling laws (Geller, 1976), the total duration of rupture, τ_R, grows linearly with rupture length L, while M_0 grows as L^3, suggesting the relation

$$\tau_R = 4.8 \times 10^{-6} \times M_0^{1/3} \quad (7)$$

(with M_0 in N m and τ_R in s), which corresponds to a rupture velocity $V_R = L/\tau_R \approx 3.45\,\mathrm{km\,s^{-1}}$, and is used by the Harvard CMT project to describe the source duration of small earthquakes for which it cannot be resolved by the inversion algorithm. Note that Nakanishi and Kanamori (1982) have proposed the slightly 'longer' constant 7.4×10^{-6} in (7).

The effect of source finiteness can be taken into account in the inversion by evaluating the scalar moment M_0 at each step of the inversion, inferring a duration τ_R from (7), and correcting the spectral amplitudes using the classical directivity function

$$F(\omega, \theta) = \mathrm{sinc}\left[\frac{\omega\tau_R}{2}\left(1 - \frac{V_R}{C}\cos(\theta - \phi_R)\right)\right] \quad (8)$$

where C is the phase velocity, θ the azimuth to the station, and ϕ_R the azimuth of the propagation of rupture, which can be taken as the fault strike ϕ. The choice of fault strike among the four possible candidates (conjugate mechanisms and 180° indeterminacy on ϕ) is left to the operator, and can proceed by trial and error, so as to optimize the convergence of the inversion.

In addition, and as detailed for example by Geller (1976), propagation along source width, as well as the finite rise time τ_r of the source, could influence spectral amplitudes. In practice, however, we found that except for the largest earthquakes studied in Section 4 (1996 Biak; 1998 Balleny) source finiteness could be neglected without leading to a degradation of the solution. The rise time τ_r is on the average four times smaller that the rupture time τ_R, and its effect is even weaker. Given that we use periods >90 s, and as long as 300 s, this empirical result is easily explained from the theoretical curves on Fig. 4 of Geller (1976), which show that the first corner frequency of the source will reach 0.01 Hz only for $M_0 \approx 10^{21}$ N m.

2.3. Performance of solutions

For each earthquake studied, we compare our results to several published moment tensor solutions: the Harvard centroid moment tensor catalog (HRV), as published regularly by Dziewonski and Woodhouse (1983 and subsequent quarterly updates), and the USGS moment tensor catalog, as listed regularly in the weekly PDE Bulletins. It is well known that those solutions can differ, occasionally even to a significant degree, on account of the different nature of the seismic waves used in the two methods (Dziewonski et al., 1981; Sipkin, 1982). In addition, we also include the 'QUICK CMT' solutions ('HRVQ') posted on their web site by the Harvard group in the immediate aftermath of the earthquakes: because of the generally smaller number of stations used, the HRVQ moments and geometries can differ from the final solutions published after a few months' delay.

Comparisons between focal mechanisms are carried out by computing the smallest angle, Ω, of the four possible Euler rotations between the two mechanisms, using the algorithm of Kagan (1991). We will call Ω the Kagan angle between the two solutions. It vanishes when the two mechanisms are the same, and reaches 120° when they differ most, i.e. when their three principal axes are permuted circularly. Scalar moments are compared by computing the logarithmic residual between them: $r = \log_{10} M_0/M_0'$.

2.4. The case of deep earthquakes

Our inversion strategy is not expected to work adequately in the case of deep earthquakes for several reasons. As discussed by Okal (1990), the Love spectra of deep earthquakes are expected to be heavily contaminated by overtones, traveling at a group velocity similar to that of the fundamental branch, and thus, inseparable in the time domain. As a result, spectral amplitudes of Love waves cannot be utilized unambiguously in the inversion. In addition, the exponential decay of the Rayleigh wave eigenfunction with depth leaves only the lowest part of the frequency spectrum adequately excited. For this reason, we restrict the computation of mantle magnitudes M_m to $T \geq 190$ s for deep earthquakes (Okal, 1990). As a result, in the case of deep earthquakes, the dimension of the data space will be strongly reduced, and the inversion becomes

unstable. While the occasional deep earthquake could be successfully inverted, our experience has been that our method could not be applied consistently and reliably to sources deeper than 200 km.

3. A case study: the 1995 Mexican earthquake

In this section, we use the Guerrero, Mexico earthquake of 14 September 1995 as a case study for which we carry out a large number of systematic tests, in which we vary many inversion parameters, our goal being to evaluate a threshold of robustness for the solution when the dimension of the dataset is systematically decreased. We performed a total of more than 200 inversions of Love and Rayleigh spectral amplitudes. The first rows of Table 1 gives the HRV, HRVQ and USGS best-double-couple solutions for the 1995 Mexican earthquakes.

We use very long-period channels at eight GEOSCOPE stations, shown on Fig. 1, and covering an effective azimuth range of 92° (within the 180° window resulting from the azimuth indeterminacy inherent in the method). Epicentral distances range from 46° (KOG) to 155° (RER). The Love record at KOG was discarded.

The 15 individual records were processed through TREMORS, a one-station algorithm (Reymond et al., 1991) for the automatic detection of a teleseismic event, its location and the evaluation of its seismic moment using the mantle magnitude calculation of Okal and Talandier (1989). All values of ground motion spectral amplitudes at periods between 70 and 300 s were retained (after equalization to a distance Δ=90°). For each individual record, the spectrum was smoothed by best-fitting a cubic spline in the frequency-log(amplitude) plane. The resulting spectra then constitute the database to be inverted.

We first proceeded to invert the dataset of eight Rayleigh waves in the period range 90–190 s. The first stage of the inversion, equivalent to Romanowicz and Suárez' (1983) first step, yields a thrust faulting mechanism (ϕ=111°; δ=45°; λ=90°) at an optimal depth of 35 km. Note that the azimuth ϕ is remarkably close to that of the HRV solution (115°), while the inverted depth is somewhat greater than found in all three published CMTs; however, depth resolution is only weak (see Fig. 2). The second stage of the inversion converges on the solution ϕ=128°; δ=65°; λ=115°. It is straightforward to reject the two possible normal faulting solutions (ϕ=128 or 308°; δ=65°; λ=295°), for example on the basis of a sharp dilatational P wave at PPT identified as part of the automated TREMORS processing. As for the other thrust faulting solution (ϕ=305°; δ=65°; λ=115°), it is considered less likely in the local tectonic context involving shallow angle subduction of the Cocos Plate under Central America. Fig. 3a shows the fit of spectral amplitudes at selected periods.

The Kagan angles between the PDFM solution and the published ones are summarized in Table 1. The PDFM solution is rotated 22° from HRV; this angle is almost exactly the median rotation (21°) for the dataset common to the entire USGS and HRV catalogs (Frohlich and Davis, 1999), and thus, our solution can be considered good. The inverted scalar moment, M_0=1.18×10^{20} N m is 0.90 times the HRV value. The difference, r=0.05 logarithmic units, can be regarded as insignificant given the general precision with which seismic moments are determined. As a first conclusion of this section, the inversion, still limited to Rayleigh waves, yields an acceptable solution for the moment tensor. We call this solution the PDFM solution, and keep it as a reference for comparison with other inversions.

We then explore the robustness of the inversion when its parameters are varied. Table 1 keeps track of all results, notably through the Kagan angles of the solutions both with HRV, and with the reference PDFM solution.

3.1. Depth

We start by varying the constrained depth at which the inversion is performed, in this case from 5 to 65 km. As shown on Fig. 2 and in Table 1, a moderate increase in depth has little effect on the quality of the solution, which starts to diverge only at 65 km. On the other hand, very shallow sources lead to a quick deterioration of the solution. As a result of the node in Q_R at the surface, a singularity develops and the inversion returns essentially a vertical dip-slip (δ=90°; λ=90°) of large amplitude (note the near trebling of the scalar moment at 5 km), a geometry known to excite virtually no energy at all into the seismograms.

Table 1
Moment tensor solutions for the Mexican earthquake of 14 September 1995

Description	Depth (km)	Moment (10^{20} N m)	Focal mechanism			Kagan angles	
			ϕ (°)	δ (°)	λ (°)	HRV (°)	PDFM (°)
Catalog solutions							
HRV-Harvard final	21	1.31	115	75	95		22
HRVQ-Harvard QUICK	15[a]	1.77	114	79	91	6	28
USGS	23	1.4	115	75	106	11	17
Solutions from this study: Rayleigh only							
PDFM reference solution eight stations Rayleigh only	35	1.18	128	65	115	22	
Depth fixed at 5 km	5	2.80	212	84	88	99	90
Depth fixed at 15 km	15	1.11	201	83	89	88	85
Depth fixed at 25 km	25	1.10	149	73	117	35	22
Depth fixed at 45 km	45	1.22	118	64	104	14	11
Depth fixed at 55 km	55	1.13	114	63	85	15	27
Depth fixed at 65 km	65	1.20	86	79	36	59	76
Moved 10°N	35	1.04	125	65	106	16	8
Moved 10°S	35	1.30	122	64	114	21	5
Moved 10°W	35	1.13	125	63	118	25	5
Moved 10°E	35	1.13	131	68	106	18	11
PDFM T=90–190 s	35	1.18	128	65	115	22	
T=70–300 s	35	1.13	124	66	110	17	5
T=70–190 s	35	1.37	121	70	110	15	8
T=90–300 s	35	1.15	128	66	112	20	3
T=110–190 s	35	1.19	132	64	121	28	6
T=130–190 s	35	1.29	136	65	126	32	10
T=98 s	35	1.09	132	61	119	28	6
T=142 s	35	1.01	142	64	126	35	14
T=256 s	35	5.22	128	86	98	17	27
Six stations Rayleigh only CAN, INU, KOG, PPT, RER, SSB	35	1.19	132	66	117	24	4
Four stations Rayleigh only INU, KIP, NOU, SSB	35	1.09	121	61	107	18	9
Three stations Rayleigh only INU, KOG, SSB (92°)	35	1.02	131	63	102	19	15
Two stations Rayleigh only RER, SSB (60°)	35	1.37	117	60	115	25	12
Damped inversion, ε^2=30	35	1.06	129	62	116	25	3
Solutions from this study: Love included							
Eight Rayleigh; seven Love (T=90–190 s)	35	0.97	130	70	101	15	15
Eight Rayleigh; seven Love (T=90–300 s)	35	0.96	128	68	100	14	15
Eight R; seven L; Damped (ε^2=30)	35	1.10	120	72	93	7	22
Eight R; seven L; 15 km	15	1.55	48	87	80	67	80
Eight R; seven L; 55 km	55	1.21	115	63	89	13	23
Eight R; seven L; moved 10°N	35	1.08	115	70	93	5	21
Eight R; seven L; moved 10°S	35	1.19	105	74	82	14	34
Eight R; seven L; moved 10°E	35	0.96	132	69	102	18	16
Eight R; seven L; moved 10°W	35	0.97	129	70	103	15	14
Four stations, R and L INU, KIP, PPT, SSB, 90–190 s	35	1.25	116	62	88	15	24
Three stations, R and L INU, KIP, SSB (92°), 90–190 s	35	1.04	112	64	85	15	27
Three Rayleigh; two Love INU, KOG, SSB (92°), 90–190 s	35	1.05	131	64	103	18	13

Table 1. (*Continued*)

Description	Depth (km)	Moment (10^{20} N m)	Focal mechanism			Kagan angles	
			ϕ (°)	δ (°)	λ (°)	HRV (°)	PDFM (°)
Two stations, R and L INU, SSB (88°), 90–190 s	35	1.03	124	63	97	15	17
Depth varied	55	1.28	135	62	103	22	16
Depth varied	25	1.29	141	78	102	26	25
Moved 10°N	35	1.12	142	73	105	26	22
Moved 10°S	35	1.12	131	72	101	15	17
Moved 10°E	35	1.12	145	73	106	29	23
Moved 10°W	35	1.12	134	72	104	19	16
Two stations, R and L KIP, SSB (61°), 90–190 s	35	0.99	122	63	93	15	20
Two stations, R and L KIP, CAN (46°), 90–190 s	35	1.74	92	80	81	25	43
Two stations, R and L KIP, NOU (35°), 90–190 s	35	2.02	92	78	87	23	40
Two stations, R and L NOU, SSB (27°), 90–190 s	35	2.25	70	85	80	46	62

[a] Depth constrained in Harvard QUICK inversion.

3.2. Epicentral location

We examine here the influence of an erroneous epicentral location on the results of the inversion. As discussed above, we are motivated by the fact that initial epicentral estimates obtained in real time, for example through the TREMORS algorithm (Reymond et al., 1991), can have significant errors, on the order of a few hundred km. In this context, we conduct four tests in which we artificially move the epicenter by perturbing its latitude or longitude by ±10°. The magnitude of this displacement of the epicenter was selected as a worst case scenario for any realistic real-time condition. However, it may be more relevant to the case of historical earthquakes for which reported epicenters can be grossly inaccurate (Huang et al., 1994).

The results displayed in Table 1 and on Fig. 4 show that the solution is in all cases remarkably robust, being rotated at most 11° from the reference mechanism obtained at the true epicenter. This result means that a reasonable moment tensor solution can be inverted from spectral amplitudes even when using a mediocre estimate of the earthquake's epicenter. It underscores the fundamental difference with spectral phases, which would be affected a minimum of 200° at 300 s, more at shorter periods, by a similar error in distance.

3.3. Frequency band

Next, we proceed to vary the frequency band over which the inversion is carried out. As documented in Table 1, the inversion is remarkably robust when the frequency band is as narrow as 1.5 mHz (T=130–190 s; actually 142–183 s because of discrete sampling). We even explored the possibility of inverting a single frequency. For eight stations well sampled in azimuth, the inversion remains stable at the shorter period (T=98 s), but diverges at the longer one (T=256 s). The latter result is easily understood since, at this long period, the source can be regarded as surficial, which triggers the Q_R singularity: the solution picks up spurious M_{xz} and M_{yz} components, and flips into a nearly pure dip-slip (δ=86°; λ=98°) of unrealistic amplitude, with M_0 reaching four times the HRV value.

3.4. Number of stations

Next, we study the influence of a reduction in the number of stations. We ran all 70 possible combinations of four stations in the dataset, as well as all 56 combinations of three. In the former case, we found only seven geometries for which the inversion either failed to converge, or yielded a grossly erroneous solution. In all such cases, several stations shared practically the same effective azimuth (e.g. the trio KOG, KIP, RER (all within 6°), or the two doublets RER, KIP (0.15°) and CAN, PPT (0.55°); Fig. 1), thus, essentially reducing the number of sampled azimuths to two. Similarly, nine of the three-station inversions failed, all of them involving two among the three stations KIP, KOG, RER. Since space limitations prevent listing the entire set of solutions, we simply present in Table 1 representative cases for which the inversion

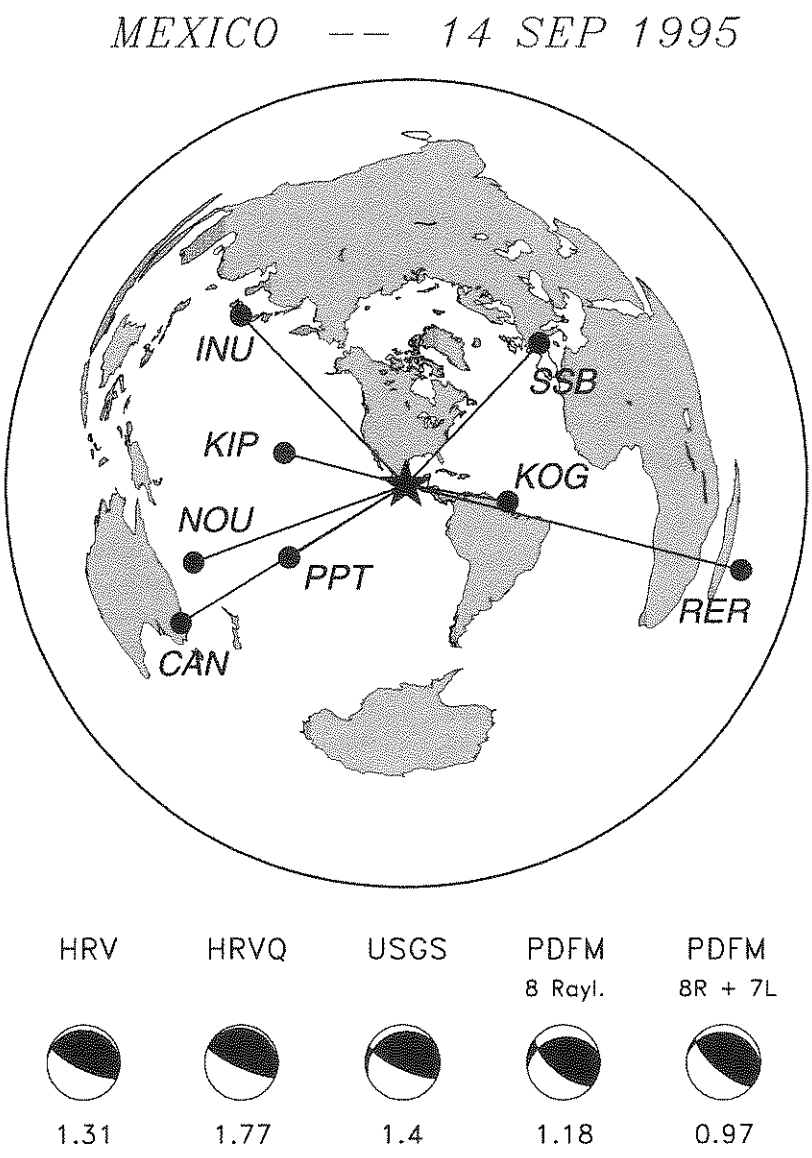

Fig. 1. Map of the case study of the 1995 Guerrero, Mexico earthquake. This is an azimuthal equidistant projection centered at the event, showing the distribution of the eight GEOSCOPE stations used. Inversion results are shown at the bottom for published solutions (HRV, HRVQ, USGS) and PDFM inversion, using either eight Rayleigh or eight Rayleigh and seven Love amplitude spectra. Scalar moments, in units of 10^{20} N m, are shown below each beachball.

converges to an acceptable solution, which we define as having a Kagan angle to the PDFM reference solution of $<30°$; the azimuth window sampled is given in parentheses.

The 28 possible two-station combinations yielded variable results, with 16 achieving stable and acceptable solutions, one of them documented in Table 1. Because of the large proportion of failures, we do not consider it feasible to routinely use two-station inversions of Rayleigh spectra, and the conclusion of this test is therefore that a minimum of three stations well distributed in azimuth is necessary for a stable and reliable inversion. The results can then be regarded as practically unaffected by the depletion of the dataset.

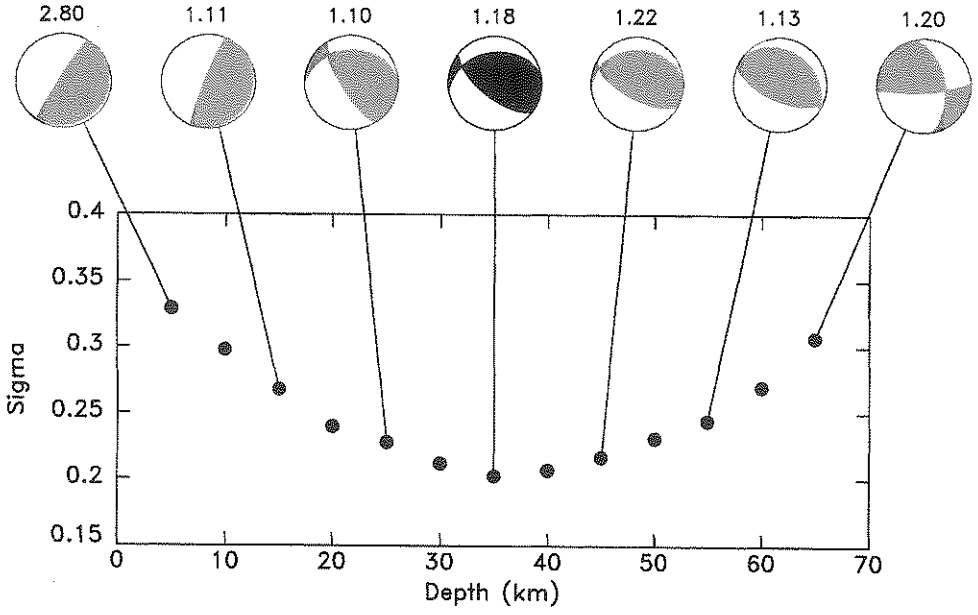

Fig. 2. Influence of depth on the inversion. The individual dots show the variation of the quality of the solution, as measured by the rms residual achieved upon convergence, as a function of the depth at which the source is constrained. Resulting focal mechanisms are also shown in gray, with the reference PDFM solution (at 35 km) shown in black. The numbers on top of the beachballs are scalar moments in units of 10^{20} N m.

3.5. Damping

All above inversion were performed without damping (ε=0 in (6)). The effect of finite damping was investigated by re-running the PDFM inversion with a damping coefficient ε^2=30 [cm^2 s^2/10^{20} N m]^2, or approximately 1% of the largest eigenvalue of $[\boldsymbol{A}^{\mathrm{T}}\boldsymbol{A}]^{-1}$ of the undamped PDFM inversion. As documented in Table 1, the introduction of this level of damping has a negligible effect on the solution, which is expected because of the nature of the mechanism (low-angle thrust faulting).

3.6. Love waves

We then proceed to include in the dataset the Love wave spectra (except at KOG where the Love amplitude is clearly deficient, probably due to instrumental noise). We did not attempt to invert Love spectral amplitudes alone, since Love waves are not excited by the component M_{zz} (see Eq. (5)), and any such inversion would require further degrading the dimension of the model space to four.

As shown in Table 1, the solution is slightly improved through steepening of the fault plane and reduction of the strike-slip component, bringing it within 15° of HRV. A broader period range (T=90–300 s) is practically without further effect. We note, however, a reduction in the scalar moment to just under 10^{20} N m. The fit of spectral amplitudes is shown in Fig. 3b. Damping (ε^2=30 units or 1% of λ_{max}) brings the solution in excellent agreement with HRV, the Kagan angle being as small as 7°.

The next entries in Table 1 show that including Love waves has practically no effect on the influence of depth on the inversion, since for shallow sources Q_L vanishes, like Q_R for Rayleigh waves, and the undamped solution becomes unstable. Because of the low-angle thrust faulting nature of the mechanism, damping cannot be expected to improve the solution at very shallow depths.

As for the influence of an erroneous epicenter, Table 1 shows that displacing the epicenter 10° to the South does change the solution substantially (it rotates 34° from PDFM and 25° from the Love–Rayleigh solution at the correct epicenter), but keeps it close

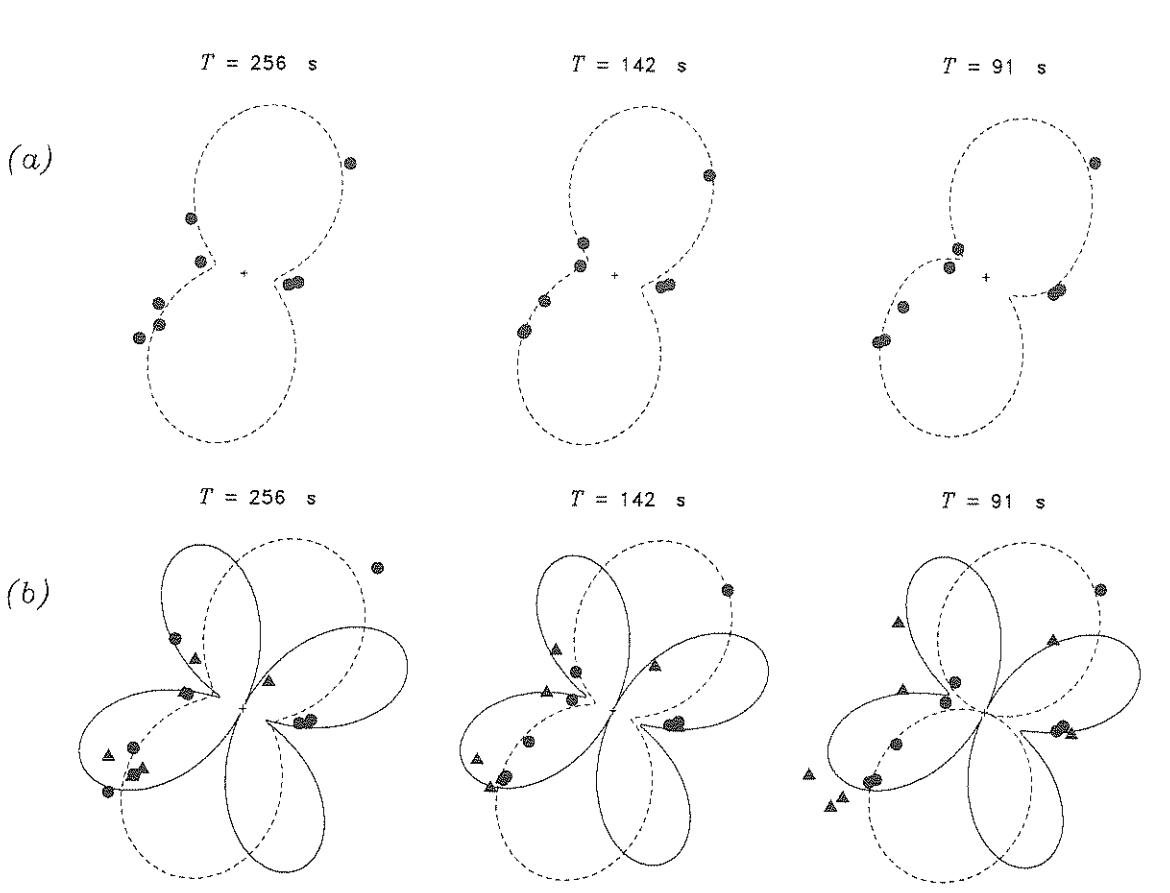

Fig. 3. Quality of fit of spectral amplitudes in the case of the 1995 Mexican earthquake: (a) inversion from Rayleigh waves only; at the three representative periods, the dashed lines are the theoretical spectral amplitudes computed from the reference PDFM mechanism, plotted as a function of azimuth, and the solid dots the observed amplitudes at the eight stations shown on Fig. 1. (b) Same as (a) after inclusion of Love waves (solid lines and triangles).

to the HRV solution. Solutions at the other displaced epicenters are found to be much more robust.

An explanation for this pattern may be sought in the azimuthal radiation patterns of the spectral Love and Rayleigh amplitudes as given by (1) and (5). As is well known (Kanamori and Stewart, 1976; Kanamori and Given, 1981), the latter are intricate functions of focal mechanism, depth, and frequency, illustrated on the left part (a) of Fig. 5 in the geometry of the PDFM mechanism of the Mexican earthquake. When the epicenter is moved, distances to stations in the direction of displacement, and azimuths to stations at right angle to that direction will be most affected. The dependence of spectral amplitudes on distance is generally weak, both for Love and Rayleigh waves. The dependence on azimuth will be controlled by the derivatives of the radiation pattern with respect to azimuth. In the case of Rayleigh waves, the isotropic coefficient S_R in (2) acts to smooth the radiation pattern into a Figure 8 shape with only weak nodes; its absence for Love waves results in a nearly perfect cloverleaf with pronounced nodes, especially at long periods. As a result, and as shown on Fig. 5b, azimuthal derivatives for Love waves (solid lines) are on average twice as large as their Rayleigh counterparts (dashed lines), whereas the spectral amplitudes are comparable (Fig. 5a).

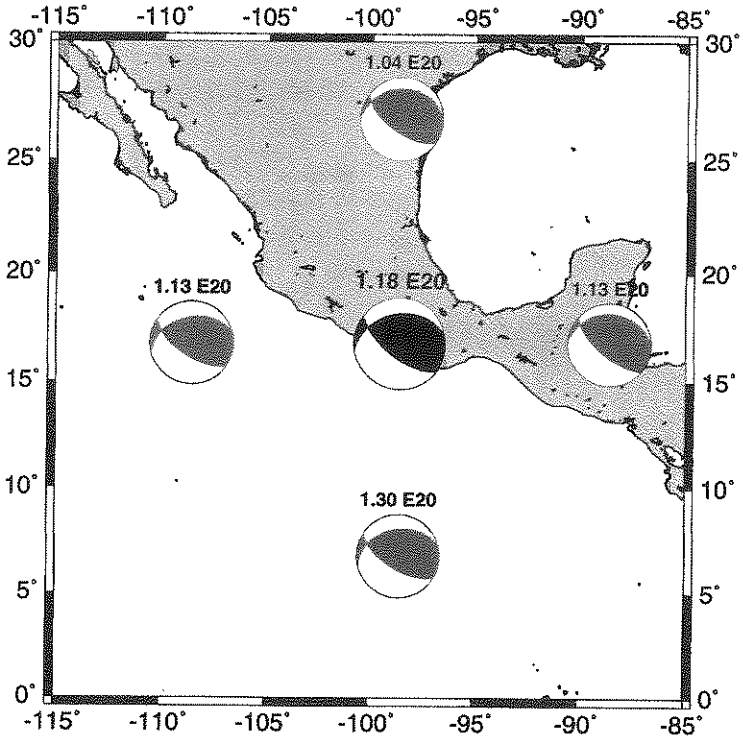

Fig. 4. Influence of epicentral mislocation on the inversion for the Mexican earthquake. The four displaced solutions are plotted at the relevant constrained epicenters, with scalar moments printed.

Finally, given the particular repartition of the stations, East–West displacements of the epicenter result in generally smaller changes in azimuth (see squares on right-center frame) than do North–South ones (see triangles on right-bottom frame), especially at stations for which the Love azimuthal derivatives are substantial (KIP, RER). This results in the observed pattern of a greater sensitivity of the solution to the displacement of the epicenter to the South. However, once again, we wish to stress the extreme amplitude of the error in epicenter used in this test.

Finally, we investigated the influence of a reduced number of stations by exploring if the inclusion of Love waves into the dataset can stabilize two-station inversions to the point of making them reliable. Of the 21 possible combinations, six failed to converge to a satisfactory mechanism, five of those featuring a difference of effective azimuth of $<15°$. Table 1 gives several examples of successful two-station Love-and-Rayleigh inversions. Thus, the inclusion of Love waves can significantly improve the inversion of very depleted datasets, but they are found to be less robust than Rayleigh waves to epicentral inaccuracy.

We also took this opportunity to explore the effect of inaccuracies in depth or epicenter on inversion from very depleted datasets, using the particular case of the INU-SSB Love and Rayleigh combination. As might have been expected, a strongly depleted dataset fares less well than a larger one when the spatial parameters of the source are erroneous, but the quality of the solution remains acceptable, as documented by Kagan angles with respect to the reference solutions in the 15–30° range.

The conclusion of this exhaustive experiment on the 1995 Guerrero earthquake is that the PDFM method can provide reliable estimates of the moment tensor, even when the parameters of the inversion are changed, and in particular when the number of stations is strongly reduced. Three-station inversions of Rayleigh amplitudes, or two-station inversions of Love and Rayleigh combinations are feasible when a sufficient range of effective azimuths is sampled. The listings in

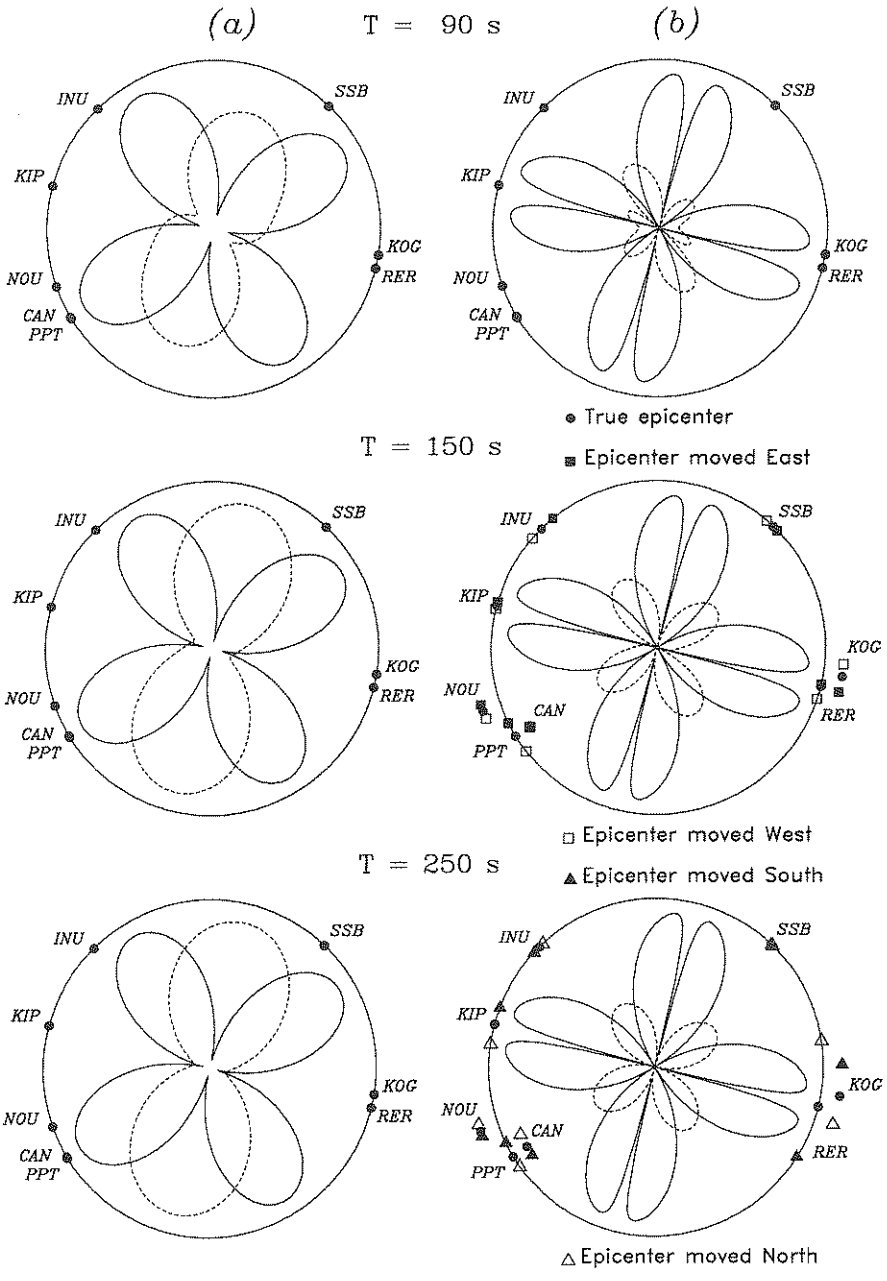

Fig. 5. (a) Azimuthal radiation patterns for surface wave spectral amplitudes at three representative mantle periods. The geometry used is that of the PDFM solution for the 1995 Mexican earthquake, with azimuths to the stations shown as solid dots. Solid lines: Love waves; dashed lines: Rayleigh waves. (b) Azimuthal derivatives of the radiation patterns. Each line in (b) is the derivative of its counterpart in (a) with respect to azimuth. Note the generally larger amplitude of the Love wave derivatives, as compared to Rayleigh waves. On the center and bottom frames, the additional symbols show variations in azimuth for each station when the epicenter is moved 10°N (open triangles), 10°S (solid triangles), 10°E (solid squares) or 10°W (open squares). In order to enhance clarity, the East and West displacements of the epicenter are shown on the center frame, the North and South ones on the bottom frame. Also, stations NOU and KOG have been moved slightly outwards, and station CAN inwards, to distinguish their symbols from those of PPT and RER, kept on the unit circle. Radial scales are arbitrary in each frame, but common to Love and Rayleigh waves.

Table 1 would suggest that results are robust beyond an azimuth window of 60° and deteriorate markedly for a window of 27°. The intermediate azimuth windows (e.g. 35° for KIP, NOU) yield acceptable geometries, but inflated values of the scalar moment. The threshold of 60° suggested by the present study coincides with the value proposed by Dufumier and Cara (1995) for a three-station inversion of the full complex spectrum.

4. Application to an extended dataset

In this section, we apply the PDFM technique, as described above, to a dataset of 43 major earthquakes between February 1996 and December 1999. Our event selection was based on a number of criteria. First, and because the PDFM technique is being developed in the context of tsunami warning, we focus on large shallow earthquakes, but do not consider several large continental shocks (e.g. the 1997 events in Tibet, Iran or Pakistan). Next, we discard events with insufficient signal-to-noise characteristics at Papeete. Also, in the early phase of the project, we relied exclusively on TREMORS data, and our pre-1998 dataset had to suffer from significant disruption in real-time data flow. More recently, we have complemented our spectral amplitudes with values processed from GEOSCOPE and IRIS waveforms downloaded in the immediate aftermath of the events. For the purpose of testing the performance of the method at lower moments, we have also processed a number of smaller earthquakes, as well as events of intermediate depth. In this respect, the resulting dataset of 43 earthquakes does not claim completeness for moments greater than the smallest one in the dataset. Rather, and with the exception of the Michoacan, Mexico earthquake of 11 January 1997 which took place during a breakdown in TREMORS communications, the dataset is complete for shallow oceanic earthquakes at the level of 5×10^{19} N m, with many solutions inverted below that threshold. Incidentally, this figure is lower than generally accepted for the generation of a tsunami carrying significant far-field risk.

4.1. TREMORS data

TREMORS (**T**sunami **R**isk **E**valuation through seismic **MO**ment in a **R**eal-time **S**ystem) is an integrated detection and processing algorithm using a single three-component long-period seismic station linked to a personal computer. The software automatically detects and analyzes teleseismic signals, providing a real-time estimate of the epicenter and of the scalar seismic moment, through the mantle magnitude $M_m=\log_{10} M_0-13$, where M_0 is in N m. We refer the reader to Okal and Talandier (1989, 1990) for the details of the computation of M_m, and to Reymond et al. (1991), Hyvernaud et al. (1993), Schindelé et al. (1995) and Reymond et al. (1996) for technical descriptions of TREMORS.

In recent years, TREMORS has been upgraded to automatically send a limited amount of seismic data through INMARSAT-C satellite communications. Typically, these consist of ground motion spectral amplitudes for Rayleigh and Love waves, in the range 3–20 mHz (T=50–300 s), as well as relevant information on background noise levels. Such messages amount to no more than a few 10s of real numbers, which can be sent efficiently and economically to a central laboratory in the hour following the earthquake. At various times over the course of this project, the algorithm was implemented, albeit not simultaneously, at the nine stations shown on Fig. 6. The resulting spectral amplitudes constitute the data to be inverted.

4.2. IRIS and GEOSCOPE data

The TREMORS dataset was complemented for additional earthquakes by records obtained from the IRIS or GEOSCOPE data centers. The number of stations was purposely varied, in order to provide an empirical perspective on the effect of reducing the number of stations.

For each event, we list in Table 2 the moment tensor parameters of the published HRV, HRVQ and USGS solutions. As of the day of writing (22 January 2000), HRV solutions are not yet available after June 1999; the corresponding entries have been left blank in Tables 2 and 3.

The last columns of Table 2 give the scalar moment and geometry resulting from the inversion. The four-fold indeterminacy was lifted through a combined interpretation of impulsive wave arrivals as relayed by TREMORS, and of the general tectonic context of the event.

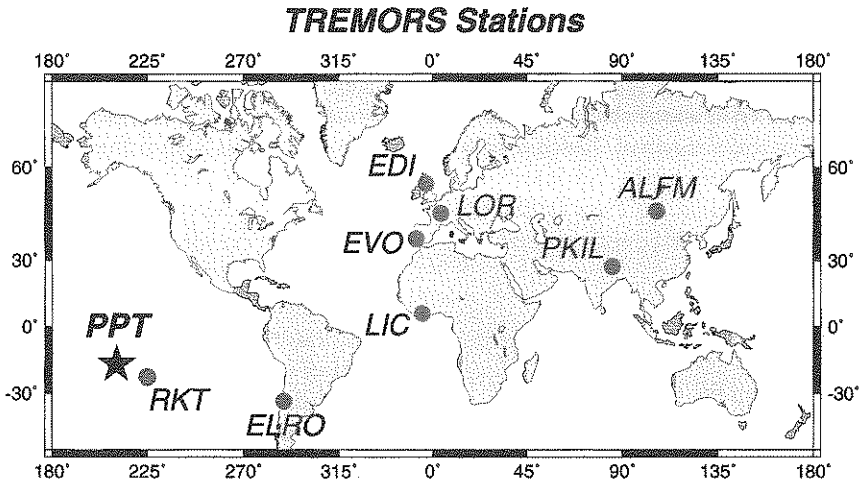

Fig. 6. Map of TREMORS-equipped stations contributing to the dataset used in Section 4. The central receiving laboratory at Papeete, Tahiti, is shown as a large star.

4.3. Results

Table 3 compares the results of our inversions (PDFM) with those of published solutions (HRV, HRVQ, and USGS). In addition, the last two sets of columns compare the USGS and HRV, and HRVQ and HRV solutions, respectively. The comparisons are expressed through the Kagan rotation angle between the two solutions, Ω, and the logarithmic moment residual, r. For example, for the first set of columns,

$$r = \log_{10} \frac{M_0(\text{PDFM})}{M_0(\text{HRV})} \tag{9}$$

The last lines of Table 3 give average values and standard deviations of the 10 sets of parameters. For comparisons involving HRV solutions, these are computed only over the first 32 events for which the final solutions have been published at the time of writing.

On average, our PDFM solutions are found to be rotated 17° away from the HRV moment tensors. This average Kagan rotation is practically equivalent to the average angle (19°) separating the USGS and HRV mechanisms in our dataset. Another perspective is given by the last column of Table 3: while the average rotation between preliminary (HRVQ) and final (HRV) Harvard mechanisms is only 9°, six events have final mechanisms rotated 15° or more away from the preliminary ones, a figure comparable to the deviations between PDFM and HRV solutions. Finally, our focal geometries are generally closer to HRV than to the USGS ones, which is not surprising given that, for large earthquakes, the HRV solutions are based primarily on mantle waves (like the PDFM ones), while USGS solutions use only body waves.

The PDFM scalar moments are also in generally excellent agreement with their HRV counterparts, the residual r being on average $\bar{r}$=0.06 logarithmic units (or a factor of 15%). This value is smaller than we reported in our previous studies on the M_m algorithm ($\bar{r}$=0.14 (Okal and Talandier, 1989) $\bar{r}$=0.07 (Hyvernaud et al., 1993)), and is, at any rate, smaller than the relevant standard deviation, σ=0.11. Fig. 7 underscores the quality of our scalar moment determinations.

In an attempt to identify any possible sources of systematic errors or bias, we present on Fig. 8 plots of various elements of our solutions. The correlation coefficients are given inside each frame; all are, at best, mediocre. We find essentially no trend between the Kagan angles and earthquake size, as measured by the HRV or HRVQ moments, whether the reference geometry is HRV, HRVQ or USGS (frames a–d). A negative correlation could have indicated the systematic influence of noise at lower sizes; a positive one that of directivity effects for the larger events. Nor do we find a trend in residual r (frame e) or absolute resid-

Table 2
Moment tensor dataset used in this study[a]

Number	Date	Epicenter		Harvard final		Harvard QUICK		USGS		PDFM (this study)			
		Lat.	Lon.	M_0	ϕ, δ, λ	M_0	ϕ, δ, λ	M_0	ϕ, δ, λ	h	M_0	ϕ, δ, λ	N_{sta}
1	07 February (038) 1996	45.29	150.45	0.64	235, 28, 113	0.65	31, 66, 80	0.48	258, 41, 124	35	0.60	229, 27, 73	4
2	17 February (048) 1996	−0.95	137.03	24	305, 80, 94	22.1	293, 79, 90	18	129, 18, 19	25	29.00	316, 83, 95	4
3	21 February (052) 1996	−9.62	−79.57	2.2	335, 14, 88	2.2	340, 15, 96	1.1	347, 4, 95	20	1.9	330, 20, 89	5
4	25 February (056) 1996	15.88	−97.98	0.55	280, 16, 74	0.35	283, 25, 82	0.54	287, 12, 84	15	0.80	280, 15, 79	4
5	29 April (120) 1996	−6.65	155.07	0.76	136, 44, 97	0.76	306, 46, 84	0.48	138, 50, 101	45	0.92	300, 43, 76	5
6	10 June (162) 1996	51.56	−177.63	8.05	248, 17, 84	8.60	259, 20, 108	7.30	211, 7, 61	25	6.35	255, 24, 84	5
7	12 November (317) 1996	−14.99	−75.68	4.60	312, 33, 55	4.40	312, 33, 52	3.70	315, 28, 58	40	4.96	324, 42, 69	3
8	21 April (111) 1997	−12.58	166.68	4.40	301, 39, 40	5.70	302, 27, 35	3.70	355, 25, 61	40	4.30	180, 68, 134	6
9	15 October (288) 1997	−30.93	−71.22	0.49	315, 12, 233	0.43	321, 12, 233	0.49	52, 15, 330	70	0.55	320, 26, 238	4
10	28 October (301) 1997	−4.37	−76.68	0.72	339, 38, 272	0.78	340, 39, 271	0.67	337, 37, 271	120	1.07	305, 67, 240	3
11	25 November (329) 1997	1.44	122.76	0.41	98, 21, 93	0.36	93, 21, 88	0.37	41, 19, 51	30	0.76	106, 23, 70	5
12	05 December (339) 1997	54.84	162.04	5.30	202, 33, 74	6.80	198, 22, 68	4.10	190, 16, 56	40	4.40	223, 38, 85	5
13	04 January (004) 1998	−22.22	170.88	1.80	348, 47, 160	1.60	346, 44, 158	1.20	307, 40, 95	110	2.20	342, 58, 160	12
14	12 January (012) 1998	−15.85	−179.38	0.12	165, 88, 173	0.11	169, 71, 186	0.12	166, 80, 186	20	0.17	167, 80, 194	6
15	30 January (030) 1998	−24.11	−70.46	0.44	8, 17, 105	0.39	29, 24, 122	0.37	41, 30, 128	30	0.37	14, 32, 111	5
16	16 February (047) 1998	52.67	−33.67	0.15	184, 70, 350	0.15	185, 75, 349	0.14	186, 54, 346	15	0.14	184, 86, 347	3
17	25 March (084) 1998	−62.88	149.53	17.00	281, 84, 17	17.00	97, 82, 332	4.60	94, 76, 352	15	23.10	103, 83, 341	8
18	01 April (091) 1998	−0.51	99.38	0.33	320, 21, 105	0.38	317, 19, 101	0.28	313, 20, 110	30	0.35	323, 20, 115	6
19	03 May (123) 1998	22.49	125.30	1.80	139, 82, 1	1.90	319, 85, 17	1.90	319, 90, 359	35	2.26	139, 73, 22	4
20	17 July (198) 1998	−2.96	141.93	0.37	287, 75, 78	0.53	289, 77, 76	0.37	302, 88, 90	35	0.49	300, 73, 78	9
21	04 August (216) 1998	−0.47	−80.05	0.64	27, 15, 124	0.50	30, 22, 121	0.42	62, 29, 150	35	0.51	210, 71, 95	6
22	09 November (313) 1998	−6.82	128.75	0.39	289, 37, 111	0.38	276, 44, 89	0.31	100, 30, 70	15	0.83	292, 14, 109	6
23	29 November (333) 1998	−2.07	124.89	4.50	92, 63, 333	3.90	95, 65, 341	4.80	106, 82, 355	10	5.06	99, 48, 355	8
24	06 December (340) 1998	1.25	126.20	0.09	201, 37, 77	0.09	214, 40, 93	0.05	238, 38, 121	30	0.12	221, 26, 96	9
25	19 January (019) 1999	−4.57	153.18	0.37	143, 31, 87	0.35	159, 30, 89	0.33	159, 31, 108	115	0.31	141, 36, 85	11
26	06 February (037) 1999	−12.80	166.65	1.11	304, 33, 41	1.20	302, 31, 37	0.88	337, 27, 70	95	1.60	332, 32, 62	10
27	08 March (067) 1999	52.07	159.57	0.26	242, 28, 101	0.21	208, 19, 88	0.27	227, 19, 97	20	0.20	222, 21, 81	6
28	20 March (079) 1999	51.57	−177.64	0.27	272, 30, 116	0.22	263, 32, 113	0.16	248, 25, 101	35	0.21	247, 31, 86	5
29	03 April (093) 1999	−16.39	−72.51	0.20	112, 20, 274	0.20	110, 20, 270	0.15	110, 20, 270	102	0.32	121, 30, 299	4
30	05 April (095) 1999	40.24	142.38	1.50	248, 17, 65	1.60	247, 18, 64	1.30	286, 18, 108	160	1.80	255, 29, 84	4
31	10 May (130) 1999	−5.17	150.92	0.47	202, 47, 235	0.54	209, 43, 237	0.49	226, 39, 247	140	0.55	215, 42, 223	13
32	15 June (166) 1999	18.40	−97.45	0.31	309, 40, 278	0.22	301, 43, 277	0.22	309, 44, 279	60	0.36	315, 36, 274	15
33	01 August (213) 1999	−30.44	−177.82			0.08	210, 17, 103	0.02	135, 38, 31	25	0.07	185, 25, 81	9
34	17 August (229) 1999	40.60	29.83			2.10	268, 84, 180	1.40	91, 76, 179	20	2.06	267, 83, 190	2
35	20 September (263) 1999	23.72	121.11			4.10	26, 27, 82	2.40	357, 29, 67	15	4.70	353, 22, 45	6
36	30 September (273) 1999	16.20	−96.87			2.00	103, 40, 262	1.40	120, 36, 259	45	2.10	116, 38, 260	3
37	16 October (289) 1999	34.60	−116.27			0.59	336, 85, 179	0.54	238, 81, 354	25	0.71	152, 85, 186	6
38	12 November (316) 1999	40.73	31.12			0.65	265, 65, 203	0.45	276, 59, 194	10	0.71	172, 65, 344	7
39	15 November (319) 1999	−1.38	88.99			0.33	13, 77, 10	0.16	98, 74, 178	20	0.44	280, 83, 158	5
40	19 November (323) 1999	−6.43	148.67			0.39	262, 28, 91	0.24	275, 37, 96	30	0.44	262, 24, 76	12
41	26 November (330) 1999	−16.45	168.18			2.00	191, 28, 105	0.93	150, 23, 48	10	2.40	185, 26, 73	13
42	06 December (340) 1999	57.32	−154.34			0.36	357, 63, 183	0.34	355, 68, 174	55	0.33	354, 62, 164	13
43	11 December (345) 1999	15.80	119.76			0.96	12, 89, 281	0.58	190, 87, 82	10	0.96	105, 18, 186	6

[a] All angles in degrees, depth h in km, all moments in 10^{20} N m.

Table 3
Comparison of moment tensor solutions

Number	Date	PDFM vs. HRV		PDFM vs. HRVQ		PDFM vs. USGS		USGS vs. HRV		HRVQ vs. HRV	
		r	Ω	r	Ω	r	Ω	r	Ω	r	Ω
1	96038	−0.03	35	−0.03	33	0.10	33	−0.12	19	0.01	2
2	96048	0.08	11	0.12	24	0.21	55	−0.12	65	−0.04	12
3	96052	−0.06	9	−0.06	6	0.24	19	−0.30	11	0.00	4
4	96056	0.16	5	0.36	10	0.17	4	−0.01	5	−0.20	11
5	96120	0.08	6	0.08	7	0.28	2	−0.20	7	0.00	1
6	96162	−0.10	10	−0.13	21	−0.06	28	−0.04	18	0.03	14
7	96317	0.03	12	0.05	13	0.13	15	−0.09	6	−0.02	3
8	97111	−0.01	12	−0.12	22	0.07	48	−0.08	40	0.11	13
9	97288	0.05	14	0.11	15	0.05	30	0.00	20	−0.06	6
10	97301	0.17	40	0.14	39	0.20	39	−0.03	2	0.03	2
11	97329	0.27	30	0.32	30	0.31	48	−0.04	22	−0.06	2
12	97339	−0.08	15	−0.19	21	0.03	26	−0.11	19	0.11	11
13	98004	0.09	13	0.14	15	0.26	52	−0.18	45	−0.05	4
14	98012	0.15	22	0.19	13	0.15	8	0.00	15	−0.04	21
15	98030	−0.08	15	−0.03	11	0.00	15	−0.08	19	−0.05	10
16	98047	−0.03	17	−0.03	11	0.00	32	−0.03	17	0.00	6
17	98084	0.13	13	0.13	12	0.70	16	−0.57	23	0.00	19
18	98091	0.03	7	−0.04	8	0.10	6	−0.07	12	0.06	2
19	98123	0.10	23	0.08	45	0.08	26	0.02	8	0.02	22
20	98198	0.12	13	−0.03	12	0.12	19	0.00	22	0.15	3
21	98216	−0.10	37	0.01	32	0.09	37	−0.18	20	−0.11	9
22	98313	0.33	23	0.34	32	0.43	51	−0.10	33	−0.01	17
23	98333	0.05	25	0.11	21	0.02	35	0.03	29	−0.06	8
24	98340	0.15	15	0.14	15	0.35	18	−0.21	27	0.01	11
25	99019	−0.08	5	−0.05	16	−0.03	14	−0.05	11	−0.02	15
26	99037	0.16	15	0.12	15	0.26	6	−0.10	17	0.03	3
27	99067	−0.11	11	−0.02	21	−0.13	12	0.02	15	−0.09	24
28	99079	−0.11	16	−0.02	16	0.12	15	−0.23	14	−0.09	7
29	99093	0.20	21	0.20	23	0.33	23	−0.12	2	0.00	2
30	99095	0.08	18	0.05	18	0.14	17	−0.06	13	0.03	1
31	99130	0.07	24	0.01	19	0.05	18	0.02	19	0.06	6
32	99166	0.06	11	0.21	18	0.21	14	−0.15	4	−0.15	8
33	99213			−0.01	12	0.49	30				
34	99229			−0.01	10	0.17	23				
35	99263			0.06	16	0.29	19				
36	99273			0.02	15	0.18	6				
37	99289			0.08	11	0.12	18				
38	99316			0.04	10	0.20	22				
39	99319			0.12	9	0.44	33				
40	99323			0.05	16	0.26	17				
41	99330			0.08	27	0.41	16				
42	99340			−0.04	18	−0.01	12				
43	99345			0.00	8	0.22	11				
Average values		0.06	17	0.06	18	0.18	23	−0.10	19	−0.01	9
Standard deviations		0.11	9	0.12	9	0.16	13	0.12	13	0.07	7

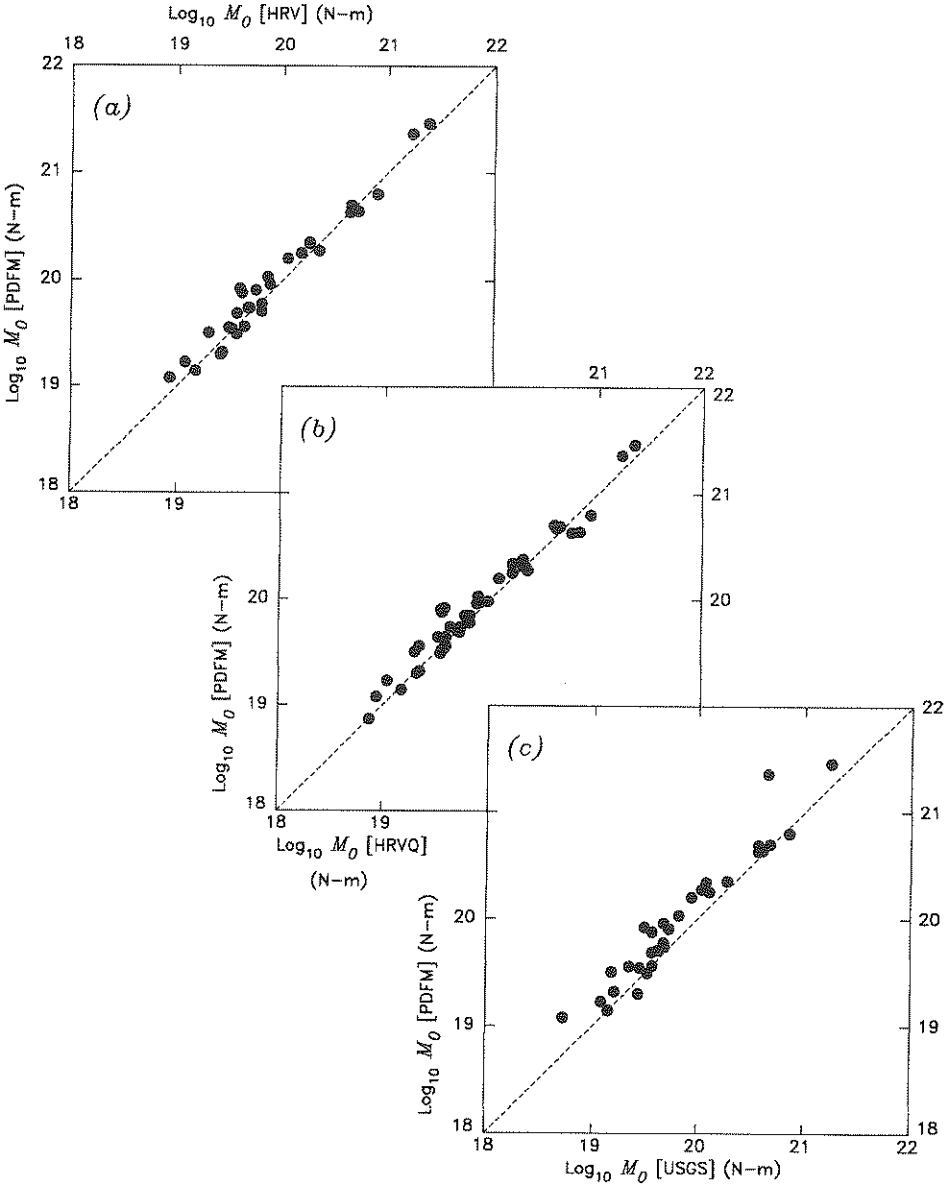

Fig. 7. Inverted values of the scalar PDFM moment vs. published moments: (a) Harvard CMT; (b) Harvard QUICK; (c) USGS.

ual $|r|$ (frame f) versus M_0. In frames g–i, we explore any possible influence of the variable number of stations on the quality of the solutions. While the largest Kagan angles are indeed found for inversions with three to six stations, some of the best solutions are obtained with similarly depleted datasets; there is no correlation between r (or $|r|$) and N_{sta}. At most, one might tentatively define a trend between $|r|$ and Kagan angle (frame j; c=0.30), expressing that, if the PDFM geometry is off by a large amount, then the scalar moment probably also is.

We conclude this study by plotting in frame k the Kagan angle of the USGS solutions relative to the HRV ones, versus seismic moment. The correlation

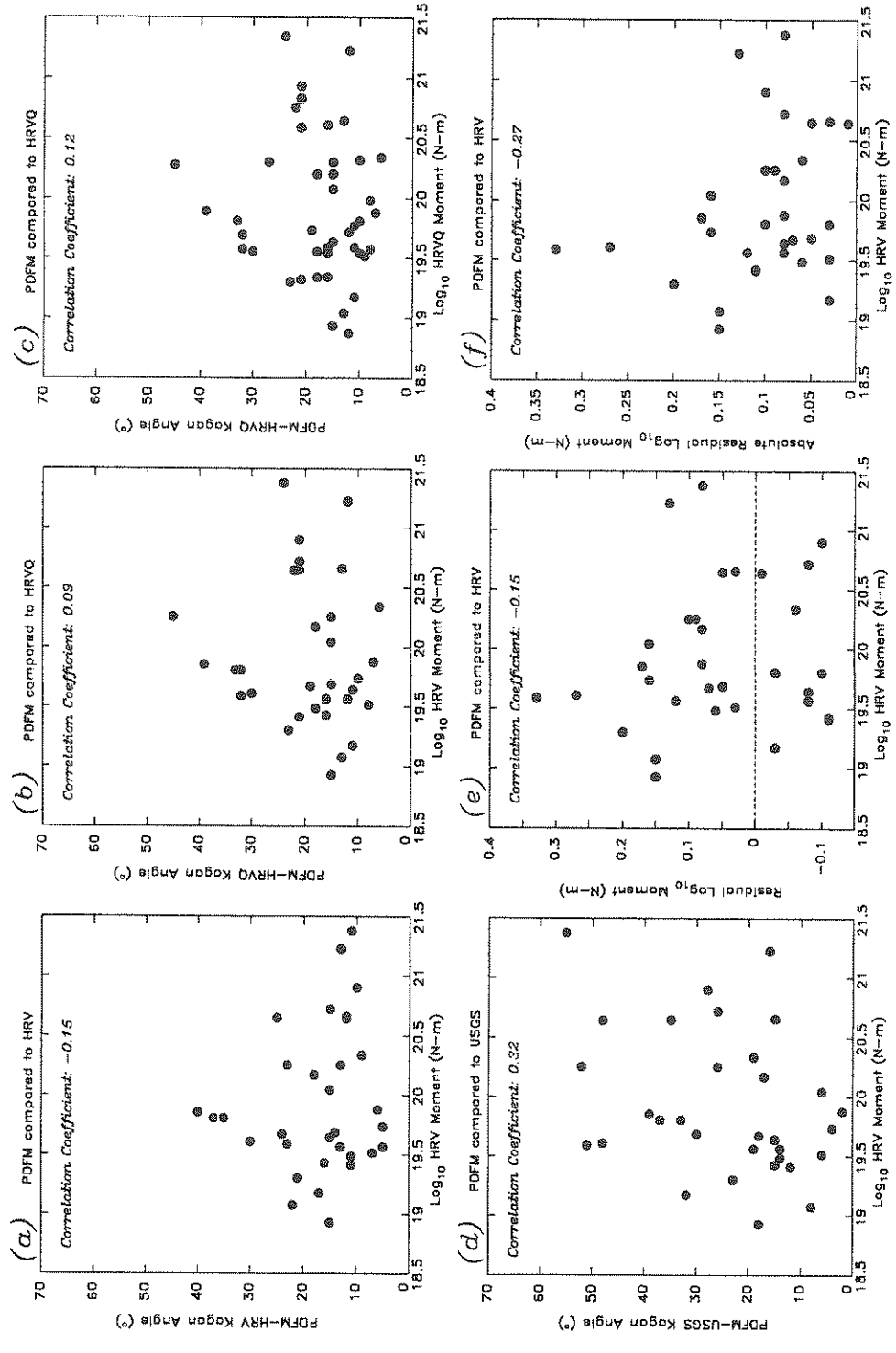

Fig. 8. Performance of the PDFM method evaluated from parameters in Table 3. (a) and (b) Kagan angle separating the PDFM and HRV (a) or HRVQ (b) solutions vs. HRV moment; (c) same as (b) plotted against HRVQ moment; (d) Kagan angle between PDFM and USGS solutions vs. HRV Moment; (e) logarithmic residual of scalar moment of PDFM solution, as compared to HRV, vs. HRV moment; (f) same as (e) for absolute value of residual, $|r|$; (g) and (h) same as (e) and (f), plotted against the number of stations used in the inversion, N_{sta}; (i) Kagan angle between PDFM and HRV vs. N_{sta}; (j) Kagan angle between PDFM and HRV solutions vs. $|r|$; (k) and (l) Kagan angles between HRV and USGS (k) or HRVQ (l) solutions vs. HRV moment.

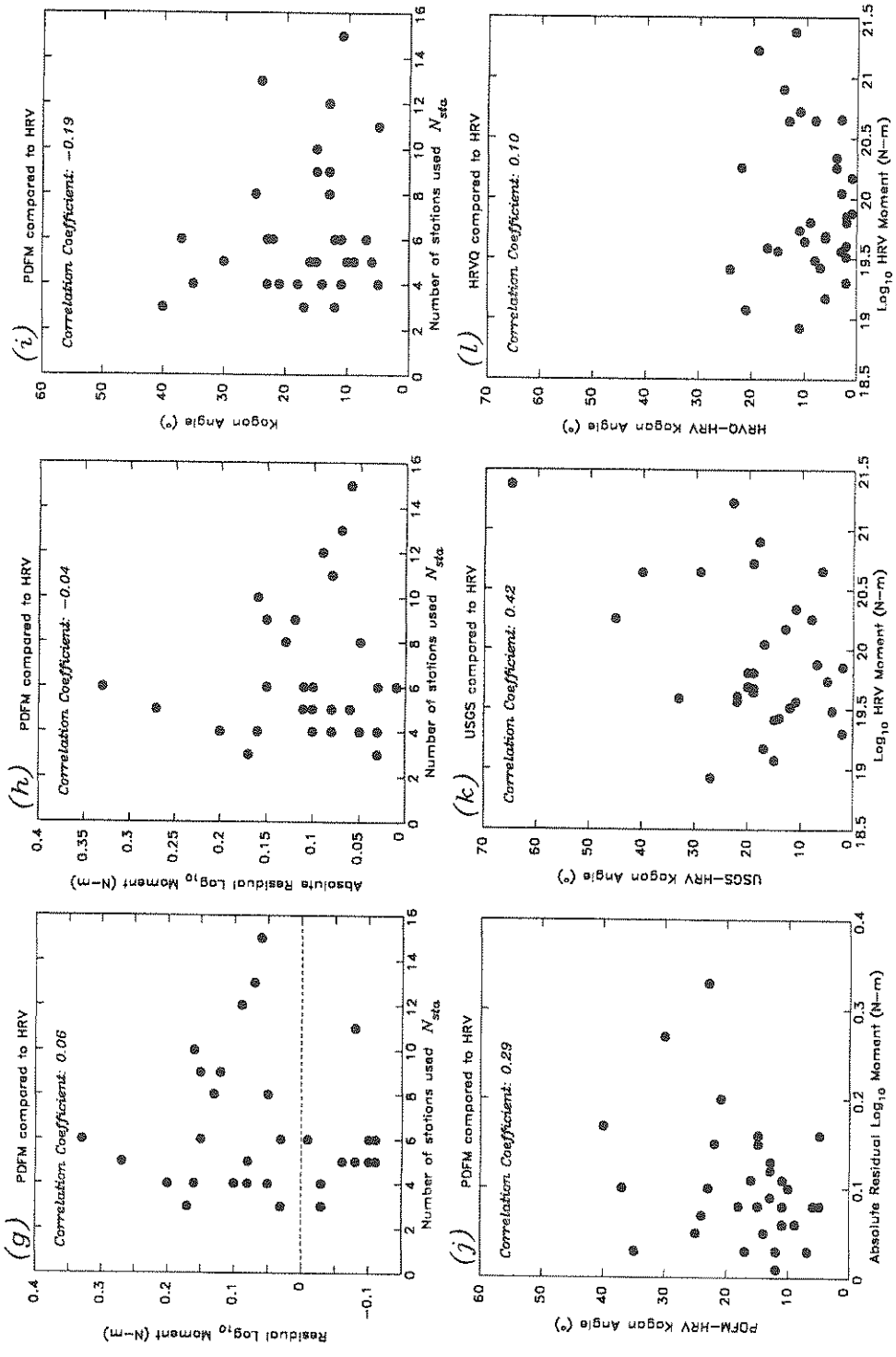

Fig. 8 (*Continued*).

coefficient, although mediocre (c=0.42) is the best in our dataset, suggesting that deviations between the two mechanisms are most significant for large earthquakes; this is easily understood, since the lower frequencies generated by those shocks are included in the HRV algorithm, but not in the USGS one. On the other hand, frame l sheds little light on the origin of the deviations between HRVQ and HRV geometries.

4.4. The case of shallow strike-slip events: the 1999 Turkish earthquake

In the case of shallow strike-slip earthquakes, such as the 1998 Balleny and 1999 Turkey events, it has been our experience that undamped inversions are most unstable. This section discusses this situation at some length, in the case of the Turkish earthquake of 17 August 1999 (a similar pattern was observed for other shallow strike-slip sources). Fig. 9 shows the distribution of stations used in our inversion, two of which, EVO and KEV, are practically nodal for Rayleigh waves. In Fig. 10, we test various inversion strategies, in an approach reminiscent of the work of Dufumier and Cara (1995).

The instability of undamped inversions stems from the non-linearity of the expression of the spectral amplitudes (3) as a function of the moment components M_{kl} (as opposed to complex spectra, which would remain linear functions of all moment components). As a result, the partial derivative of a spectral amplitude R_{ij} in (3) with respect to the dip-slip moment component M_{xz} involves not only the coefficient Q_R, which is known to be small at the surface, but M_{xz} itself. For a pure strike-slip mechanism, the latter will be close to zero, the relevant partial derivative further decreased and the singularity of the inversion enhanced, leading either to a lack of convergence or to convergence to a solution featuring spurious M_{xz} and M_{yz} components. This is observed in the first row of Fig. 10, regardless of the number of stations.

One might expect to correct this situation by performing the inversion at an arbitrarily imposed greater depth, where the excitation coefficients Q_R and Q_L

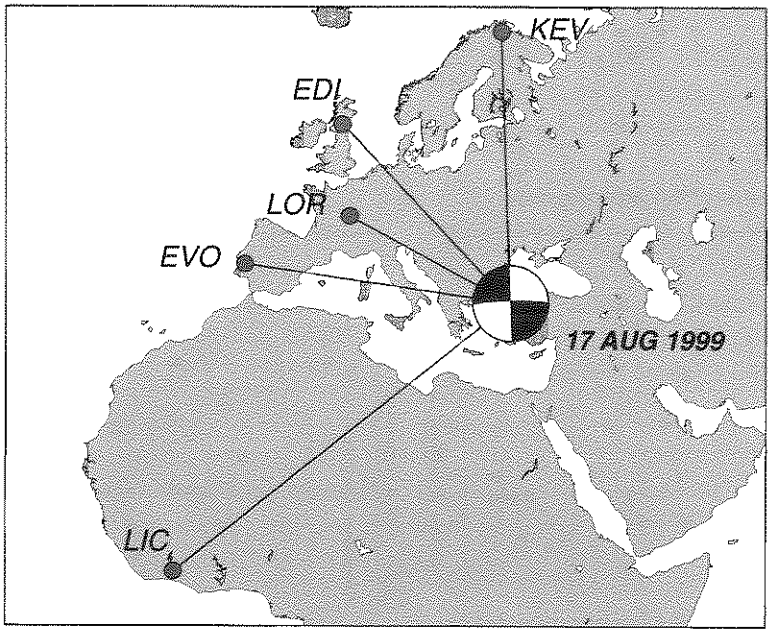

Fig. 9. Centroid moment tensor solution (HRVQ) for the Turkish earthquake of 17 August 1999. The five stations used in our inversion are shown as solid dots; note that Evora, Portugal (EVO) and Kevo, Finland (KEV) are quasi nodal for Rayleigh waves. Azimuthal equidistant projection centered at the epicenter.

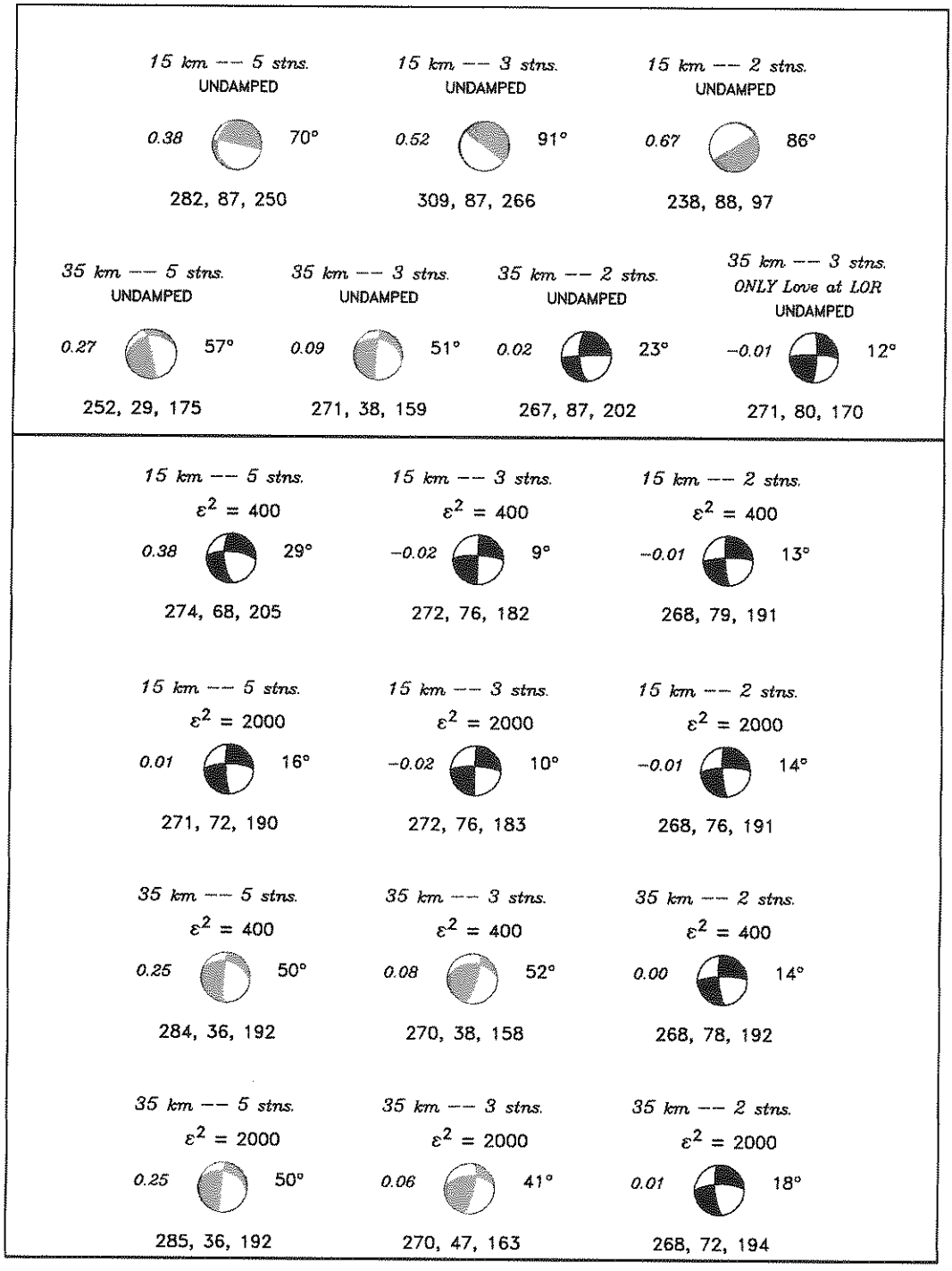

Fig. 10. Inversion results for the 1999 Turkish earthquake. Top box: undamped inversions; bottom box: damped inversions (the value of ε^2 in (6) is given in units of $[\mathrm{cm}^2\,\mathrm{s}^2/10^{20}\,\mathrm{N\,m}]^2$). For each solution, the focal geometry (strike, dip, fault in degrees) is given below the beachball, the logarithmic moment residual r in italics at left, and the Kagan angle from the HRVQ mechanism (shown on Fig. 9) at right. Two-station inversions involve only EVO and KEV; three-station ones add LOR. Gray shading identifies those solutions deemed unacceptable, on account of a Kagan angle with respect to HRVQ >30°. See text for details.

would have picked up some amplitude, especially in the higher-frequency portion of the spectrum, and thus, stabilized the inversion. However, theoretical computations show that while the strike-slip Love excitation P_L varies very slowly with depth in the crust, its Rayleigh counterpart P_R is more sensitive to depth. Thus, inversion at an erroneous depth will poorly fit the observed Love-to-Rayleigh spectral ratio with a strike-slip source and develop spurious M_{xz} and M_{yz} components (five-station inversion, second row of Fig. 10). The only exception to this pattern comes when the Rayleigh wave amplitudes are very small to start with, in which case the question of their true amplitude becomes irrelevant. This is the case if all stations are quasi-nodal for Rayleigh waves. As shown on Fig. 10, inversion at 35 km with only two stations (KEV and EVO), both nodal for Rayleigh waves, does indeed converge to a satisfactory solution (r=0.02; Ω=23°), whereas the addition of even a single station located in a Rayleigh lobe (e.g. LOR) degrades it considerably. On the other hand, if only the Love spectral amplitudes are included at the third station, the solution remains accurate.

The practical remedy for the inversion of shallow strike-slip events resides of course in adequate damping by the introduction of a non-zero ε^2 in (6). This is documented in the bottom box of Fig. 10, where inversions are carried out for various combinations of depth, number of stations, and values the damping, ε^2, given in the units of $(\partial R_{ij}^2/\partial M_{pq})^2$ in Eq. (3), namely [cm^2 s^2/10^{20} N m]^2. In practice, the coefficients S_R, P_L, P_R are expected to be on the order of a few times 1 (cm s/10^{20} N m) (e.g. Kanamori and Given, 1981), and the partial derivatives making up the matrix $\boldsymbol{A}$ in (6), a few tens to hundreds (cm^2 s^2/10^{20} N m). We have verified that the largest eigenvalues of $\boldsymbol{A}^T\boldsymbol{A}$ are in the range 10^4 [cm^2 s^2/10^{20} N m]^2; in such units, ε^2=400 then corresponds to moderate damping, bringing the condition number of the damped system (Tarantola, 1987) down to values of a few units to a few tens. Fig. 10 shows that greater damping, forcing stability at the potential price of a lack of resolution, has practically no effect on the result of the inversion.

Finally, damping restores the resolution of depth, through correct interpretation of non-zero Rayleigh spectral amplitudes, the last two rows of Fig. 10 showing that damped inversions at the greater depth lead to unacceptable mechanisms. We verified independently that the minimum residual achieved for damped inversions was indeed obtained at h=15 km.

5. Conclusion

We have established the feasibility of obtaining adequate estimates of deviatoric moment tensors in quasi-real time, from the inversion of the spectral amplitudes of mantle Rayleigh waves (with the optional addition of Love waves) at a very limited number of stations. Notwithstanding the two-fold indeterminacy inherent in this method, we were able to achieve solutions deviating from the final Harvard moment geometry in amounts no greater than the scatter among solutions derived by different methodologies. We find our method particularly robust with respect to uncertainties in epicentral location, which are inevitable under real-time operational conditions, and could bring large errors to the interpretation of the complex phase spectra. Reliable solutions, defined as rotated <30° from the Harvard CMT, can be obtained by inverting Rayleigh spectral amplitudes from as few as three stations. The introduction of Love waves can allow two-station inversions, provided that the azimuthal coverage is >60°.

While the PDFM method does not pretend to substitute for a full centroid moment tensor inversion, it can provide robust estimates of the focal geometry of large distant earthquakes, based on a very minimal amount of information, which can be transmitted efficiently and in real time, for example in the context of the development of the TREMORS system.

Our approach also has a potential application to historical earthquakes, for which we have found that station time corrections are often poorly, if at all, preserved in the archives (Huang et al., 1994); the uncertainty between relative timing at several stations then prohibits the simultaneous inversion of the full complex spectra, while the amplitude information is unaffected.

Acknowledgements

We thank Seth Stein for a discussion of inversion theory. The IRIS and GEOSCOPE data were obtained from their respective data centers. Some of the figures

were prepared using the GMT software (Wessel and Smith, 1991).

References

Aki, K., Richards, P.G., 1980. Quantitative Seismology. Freeman, San Francisco, 932 pp.

Ben-Menahem, A., 1961. Radiation of seismic surface waves from finite moving sources. Bull. Seismol. Soc. Am. 51, 401–435.

Buland, R.P., Gilbert, J.F., 1976. Matched filtering for the seismic moment tensor. Geophys. Res. Letts. 3, 205–206.

Dufumier, H., 1996. On the limits of linear moment-tensor inversion of teleseismic body wave spectra. Pure Appl. Geophys. 147, 467–482.

Dufumier, H., Cara, M., 1995. On the limits of linear moment-tensor inversion of teleseismic surface wave spectra. Pure Appl. Geophys. 145, 235–257.

Dziewonski, A.M., Anderson, D.L., 1981. Preliminary reference earth model. Phys. Earth Planet. Inter. 25, 197–256.

Dziewonski, A.M., Woodhouse, J.H., 1983. An experiment in systematic study of global seismicity: centroid moment tensor solutions for 201 moderate and large earthquakes of 1981. J. Geophys. Res. 88, 3247–3271.

Dziewonski, A.M., Chou, T., Woodhouse, J.H., 1981. Determination of earthquake source parameters from waveform data for studies of global and regional seismicity. J. Geophys. Res. 86, 2825–2852.

Ekström, G., Dziewonski, A.M., Stein, J.M., 1986. Single-station CMT: application to the Michoacan, Mexico earthquake of September 19, 1985. Geophys. Res. Letts. 13, 173–176.

Frohlich, C.F., Davis, S.D., 1999. How well constrained are well-constrained T, B, and P axes in moment tensor catalogs? J. Geophys. Res. 104, 4901–4910.

Geller, R.J., 1976. Scaling relations for earthquake source parameters and magnitudes. Bull. Seismol. Soc. Am. 66, 1501–1523.

Huang, W.-C., 1996. Centroid-moment tensor solutions from analog seismograms of deep earthquakes (1907–1976). Ph.D. Dissertation, Northwestern University, Evanston, IL, 196 pp.

Huang, W.-C., Ekström, G., Okal, E.A., Salganik, M.P., 1994. Application of the CMT algorithm to analog recordings of deep earthquakes. Phys. Earth Planet. Inter. 83, 283–297.

Hyvernaud, O., Reymond, D., Talandier, J., Okal, E.A., 1993. Four years of automated measurement of seismic moments at Papeete using the mantle magnitude M_m: 1987–1991. Tectonophysics 217, 175–193.

Kagan, Y.Y., 1991. 3-D rotation of double-couple earthquake sources. Geophys. J. Int. 106, 709–716.

Kanamori, H., Given, J.W., 1981. Use of long-period surface waves for rapid determination of earthquake source parameters. Phys. Earth Planet. Inter. 27, 8–31.

Kanamori, H., Stewart, G.S., 1976. Mode of strain release along the Gibbs fracture zone. Phys. Earth Planet. Inter. 11, 312–332.

Nakanishi, I., Kanamori, H., 1982. Effects of lateral heterogeneity and source process time on the linear moment tensor inversion of long-period Rayleigh waves. Bull. Seismol. Soc. Am. 72, 2063–2080.

Okal, E.A., 1990. M_m: a mantle wave magnitude for intermediate and deep earthquakes. Pure Appl. Geophys. 134, 333–354.

Okal, E.A., Talandier, J., 1989. M_m: a variable period mantle magnitude. J. Geophys. Res. 94, 4169–4193.

Okal, E.A., Talandier, J., 1990. M_m: extension to Love waves of the concept of a variable-period mantle magnitude. Pure Appl. Geophys. 134, 355–384.

Patton, H., Aki, K., 1979. Bias in the estimate of seismic moment tensor by the linear inversion method. Geophys. J. R. Astron. Soc. 59, 479–495.

Reymond, D., Hyvernaud, O., Talandier, J., 1991. Automatic detection, location and quantification of earthquakes: application to tsunami warning. Pure Appl. Geophys. 135, 361–382.

Reymond, D., Robert, S., Thomas, Y., Schindelé, F., 1996. An automatic tsunami warning system. Phys. Chem. Earth 21, 75–81.

Romanowicz, B.A., 1982. Moment tensor inversion of long-period Rayleigh waves: a new approach. J. Geophys. Res. 87, 5395–5407.

Romanowicz, B.A., Guillemant, P., 1984. An experiment in the retrieval of depth and source mechanism of large earthquakes using very long-period Rayleigh wave data. Bull. Seismol. Soc. Am. 74, 417–437.

Romanowicz, B.A., Suárez', G., 1983. On an improved method to obtain the moment tensor and depth of earthquakes from the amplitude spectrum of Rayleigh waves. Bull. Seismol. Soc. Am. 73, 1513–1526.

Schindelé, F., Reymond, D., Gaucher, E., Okal, E.A., 1995. Analysis and automatic processing in near-field of the eight 1992–1994 tsunamigenic earthquakes: improvements in real-time tsunami warning. Pure Appl. Geophys. 144, 381–408.

Sipkin, S.A., 1982. Estimation of earthquake source parameters by the inversion of waveform data: synthetic waveforms. Phys. Earth Planet. Inter. 30, 242–259.

Tarantola, A., 1987. Inverse Problem Theory, Methods for Data Fitting, and Model Parameter Estimation, Elsevier, Amsterdam.

Wessel, P., Smith, W.H.F. 1991. Free software helps map and display data. Eos, Trans. Am. Geophys Un. 72, p. 441; pp. 445–446.